

# Metal sandwich plates subject to intense air shocks

Ashkan Vaziri, John W. Hutchinson \*

*Division of Engineering and Applied Sciences, Harvard University, Cambridge, MA 02138, United States*

Received 22 March 2006; received in revised form 24 August 2006

Available online 6 September 2006

Dedicated to C. Fong Shih on the occasion of his 60th birthday

---

## Abstract

Recent results on fluid–structure interaction for plates subject to high intensity air shocks are employed to assess the performance of all-metal sandwich plates compared to monolithic solid plates of the same material and mass per area. For a planar shock wave striking the plate, the new results enable the structural analysis to be decoupled from an analysis of shock propagation in the air. The study complements prior work on the role of fluid–structure interaction in the design and assessment of sandwich plates subject to water shocks. Square honeycomb and folded plate core topologies are considered. Fluid–structure interaction enhances the performance of sandwich plates relative to solid plates under intense air shocks, but not as significantly as for water blasts. The paper investigates two methods for applying the loading to the sandwich plate—responses are contrasted for loads applied as a time-dependent pressure history versus imposition of an initial velocity.

© 2006 Elsevier Ltd. All rights reserved.

*Keywords:* Sandwich plates; Honeycomb core; Folded plate core; Fluid–structure interaction; Air shocks

---

## 1. Introduction

Potential advantages of all-metal sandwich plates over solid plates of equal mass have been documented in recent studies under shock loading in both air and water (Fleck and Deshpande, 2004; Rabczuk et al., 2004; Xue and Hutchinson, 2004; Rathbun et al., 2006; Liang et al., in press). Fluid–structure interaction in a water blast has been shown to significantly enhance the relative performance of a sandwich plate due to a reduction in the momentum acquired by the sandwich plate compared to that acquired by the solid plate. Fluid–structure interaction has not previously been taken into account in assessing relative plate performance in air blasts, due, on the one hand, to the fact that Taylor's (1963) linear theory for blasts suggests the effect is small and, on the other hand, to the absence of theoretical results for intense air blasts. The fluid–structure interaction theory of Taylor (1963) uses an acoustic approximation wherein the fluid is assumed to undergo relatively small volume changes. Kambouchev et al. (in press) have recently extended the Taylor theory of fluid–structure

---

\* Corresponding author.

*E-mail address:* [hutchinson@husm.harvard.edu](mailto:hutchinson@husm.harvard.edu) (J.W. Hutchinson).

interaction for air blasts by accounting for nonlinear compressibility and finite shock behavior. These results will be summarized briefly in Section 2. They will be applied to sandwich and solid plates in Section 3 to assess the role of fluid–structure interaction on the relative performance under intense air shocks. The approaches adopted make use of the new fluid–structure interaction theory of Kambouchev et al. (in press) to specify dynamic loadings on the plates, thereby decoupling the structural analysis from the analysis of the fluid.

When the response time characterizing the overall motion of a plate is long compared to the period of the blast pulse, it has been common practice to represent the loading as an initial momentum, or velocity, imparted to the plate where the momentum is obtained from the fluid–structure interaction theory. This approximation is compared with a more accurate approach that applies a time-dependent pressure history derived from the fluid–interactions theory to the plate.

## 2. Fluid–structure interaction for a plate subject to an intense air blast

Kambouchev et al. (in press) have achieved a significant extension of Taylor’s (1963) linear theory for the momentum transmitted to a plate when struck by a blast wave in air. The new theory will be referred to as KNR theory in the sequel. As in Taylor’s analysis, one-dimensional motion of the fluid and plate is considered, relevant to a planar shock wave impacting the plate. KNR theory accounts for nonlinear compressibility of the air and finite shock conditions. As in Taylor’s model, the plate is idealized as an unsupported planar surface with mass/area,  $m_P$ . Resistance from the air behind the plate is neglected. The new theory extends the formulas for the momentum transmitted to the plate into the range of intense air shocks with pressures as large as 100 MPa, but still below levels at which non-ideal gas effects such as ionization begin to become important. In this section the main findings of KNR theory relevant to the assessment of metal sandwich plates will be summarized. The fluid–structure interaction results are in the form of approximate formulas constructed to reproduce asymptotic limits and to interpolate full numerical simulations in intermediate regimes. The reader is referred to by Kambouchev et al. (in press) for details of the numerical analysis and the derivation of the approximate formulas listed below.

Denote ambient atmospheric pressure, density and sound speed by  $p_A$ ,  $\rho_A$  and  $c_A$  with  $c_A = \sqrt{1.4p_A/\rho_A}$ . The plate has mass/area,  $m_P = \rho_P h_P$ , where  $\rho_P$  and  $h_P$  are its density and thickness. The incident wave striking the plate has a shock at its front. At the instant the incident wave arrives at the plate it is characterized by an over-pressure history that decays approximately exponentially in time with time constant,  $t_0$ , i.e.  $p = p_0 e^{-t/t_0}$ . The peak over-pressure,  $p_0$ , occurs just behind the shock front; it will be used to measure the intensity of the incident blast wave and  $t_0$  is period of the incident wave. In the linear acoustic limit,  $p_0 t_0$  is the momentum/area of the incident wave, but not in the nonlinear theory. The peak density,  $\rho_0$ , just behind the shock in the incident wave is

$$\frac{\rho_0}{\rho_A} = \frac{7 + 6(p_0/p_A)}{7 + (p_0/p_A)} \quad (1)$$

and the speed of the shock front,  $c_s$ , is

$$\frac{c_s}{c_A} = \sqrt{\frac{6p_0}{7p_A} + 1} \quad (2)$$

The peak over-pressure,  $p_R$ , when the incident wave is reflected from a rigid surface (i.e. a plate with  $m_P \rightarrow \infty$ ) is the long-established result associated with shock front itself:

$$\frac{p_R}{p_0} = 2 \frac{7 + 4(p_0/p_A)}{7 + (p_0/p_A)} \equiv C_R \quad (3)$$

For small  $p_0/p_A$ ,  $C_R \cong 2$ ; while, for  $p_0/p_A \gg 1$ ,  $C_R \rightarrow 8$ .

The new result of Kambouchev et al. (in press) for the momentum/area,  $I$ , imparted to a plate of finite mass/area,  $m_P = \rho_P h_P$ , is as follows. First, in the limit for reflection from a rigid surface (i.e.  $m_P \rightarrow \infty$ , for massive plates), they find, to good approximation,

$$\frac{I_{mp \rightarrow \infty}}{p_0 t_0} = 8 - 42 \frac{p_A}{p_0} \ln \left( 1 + \frac{p_0}{7p_A} \right) \equiv \gamma_R \tag{4}$$

For plates with finite mass/area,

$$\frac{I}{p_0 t_0} = \gamma_R \left( \frac{C_R f_R}{\gamma_R} \right)^{\frac{\beta_s}{1+\beta_s}} \beta_s^{\frac{\beta_s}{1-\beta_s}} \tag{5}$$

or, equivalently,

$$\frac{I}{I_{mp \rightarrow \infty}} = \left( \frac{C_R f_R}{\gamma_R} \right)^{\frac{\beta_s}{1+\beta_s}} \beta_s^{\frac{\beta_s}{1-\beta_s}} \tag{6}$$

The mass/area of the plate appears in the ratio of time scales,

$$\beta_s = \frac{t_0}{t_s^*} \tag{7}$$

with

$$t_s^* = \rho_P h_P / (\rho_0 c_s) \tag{8}$$

The coefficient

$$f_R = \left( \frac{6p_0}{p_A} + 7 \right) \sqrt{\frac{(6 + C_R)(p_0/p_A) + 7}{(p_0/p_A + 7)((1 + 6C_R)(p_0/p_A) + 7)(C_R(p_0/p_A) + 7)}}$$

has been derived to ensure that the momentum transferred to the plate agrees with an analytical limit for very light plates. Thus, formula (5) agrees with limits for both massive and very light plates, and it coincides with Taylor’s result in the acoustic limit. The formula was found to accurately interpolate results obtained by numerical simulation over the entire range between the various limits (Kambouchev et al., in press).

It is useful to introduce a second ratio of time scales,  $\beta_A$ , based on ambient air properties. With

$$t_A^* = \rho_P h_P / (\rho_A c_A) \tag{9}$$

define  $\beta_A$  as

$$\beta_A \equiv \frac{t_0}{t_A^*} = \beta_s \left( \frac{7 + (p_0/p_A)}{7 + 6(p_0/p_A)} \right) \left( \frac{6p_0}{7p_A} + 1 \right)^{-1/2} \tag{10}$$

where the connection between the two  $\beta$ ’s follows from (1) and (2). Because  $\beta_A$  is independent of the intensity of the wave, it will be used in the sequel as the dimensionless parameter that accounts for the mass/area of the plate.

Curves of  $I/I_{mp \rightarrow \infty}$  as a function of  $\beta_A$  for fixed values of intensity as specified by  $p_0/p_A$  are presented in Fig. 1. For incident waves with pulse time,  $t_0 = 10^{-4}$  s, the range of  $\beta_A$  in Fig. 1 corresponds to steel plates with thickness greater than 1 mm, while  $p_0/p_A = 1000$  corresponds to the peak incident wave pressure  $p_0 \cong 100$  MPa. Consequently, Fig. 1 covers much of the practical range of plate thicknesses and shock pressures for shock loadings in air.

In the analyses which follow, KNR theory is employed in two ways for modeling a uniform planar wave striking a plate. The first, called the *applied pressure approach*, applies the following time-dependent pressure history to the plate surface towards the blast:

$$p = C_R p_0 e^{-t/t_R} \quad \text{with} \quad \frac{t_R}{t_0} \equiv \frac{I}{C_R p_0 t_0} \tag{11}$$

This pressure pulse has the same peak pressure as the reflected wave and transmits to the plate precisely the impulse/area,  $I$ , given by KNR theory in (5). A plot of  $t_R/t_0$  is given in Fig. 2. The second, called the *prescribed velocity approach*, assigns an initial velocity to the solid plate, or to the face sheet towards the blast for the sandwich plate, such that the initial momentum/area is  $I$  as given by (5). Justification underlying each of these

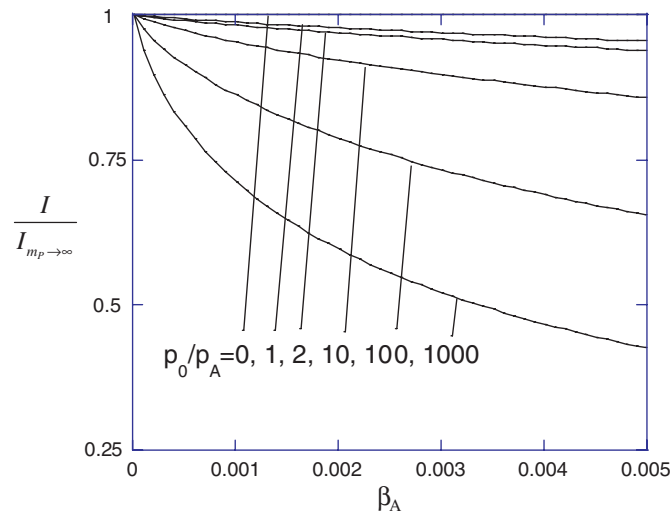


Fig. 1. Ratio of momentum/area transmitted to solid plate of thickness  $h_p$  to that transmitted to an infinitely massive plate in Eq. (4) as a function of the dimensionless measure of blast pulse duration and plate mass/area,  $\beta_A = t_0 \rho_A c_A / (\rho_p h_p)$ . The peak pressure and period of the incident pulse are  $p_0$  and  $t_0$ ;  $p_A$ ,  $\rho_A$  and  $c_A$  are the pressure, density and speed of sound in air at atmospheric pressure; and  $\rho_p$  is the density of the plate material.

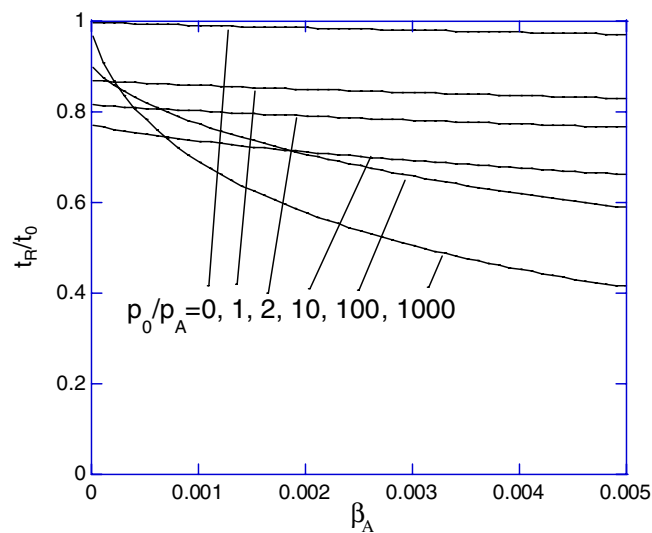


Fig. 2. Period  $t_{tr}$  of the exponential pressure history applied to the plate associated with the applied pressure approach.

approximations to a fully coupled fluid–structure computation is the short time scale of the pressure pulse,  $t_0$ , compared to the response time of the plate, combined with the fact that the early stage of the interaction between the fluid and the plate is nearly one-dimensional except where the plate is supported. Specifically, for many shocks,  $t_0 \sim 10^{-4}$  s, and the time for a meter-scale plate to reach maximum deflection is  $\approx 5 \times 10^{-3}$  s with a core crushing period intermediate between the two (Hutchinson and Xue, 2005).

### 3. Solid and sandwich plates subject to intense air blasts

In this section, simulations that employ the two approaches for applying the blast loading to solid and sandwich plates will be presented for uniform loading of plates that are infinite in one direction and are

clamped along two edges (Fig. 3). The width of the plates is  $2L$ . Two core topologies of the sandwich plates will be considered: square honeycomb and folded plate, also known as the corrugated plate.

Attention will be limited to solid and sandwich plates of the same mass/area,  $M$ , and made from the same material—304 stainless steel. The steel has density,  $\rho_P = 8000 \text{ kg m}^{-3}$ . A piecewise function has been fit to the true stress-log strain tensile behavior of the material giving

$$\sigma = \begin{cases} E_s \varepsilon, & \varepsilon \leq \sigma_Y/E \\ \sigma_Y (E\varepsilon/\sigma_Y)^N, & \varepsilon > \sigma_Y/E \end{cases} \quad (12)$$

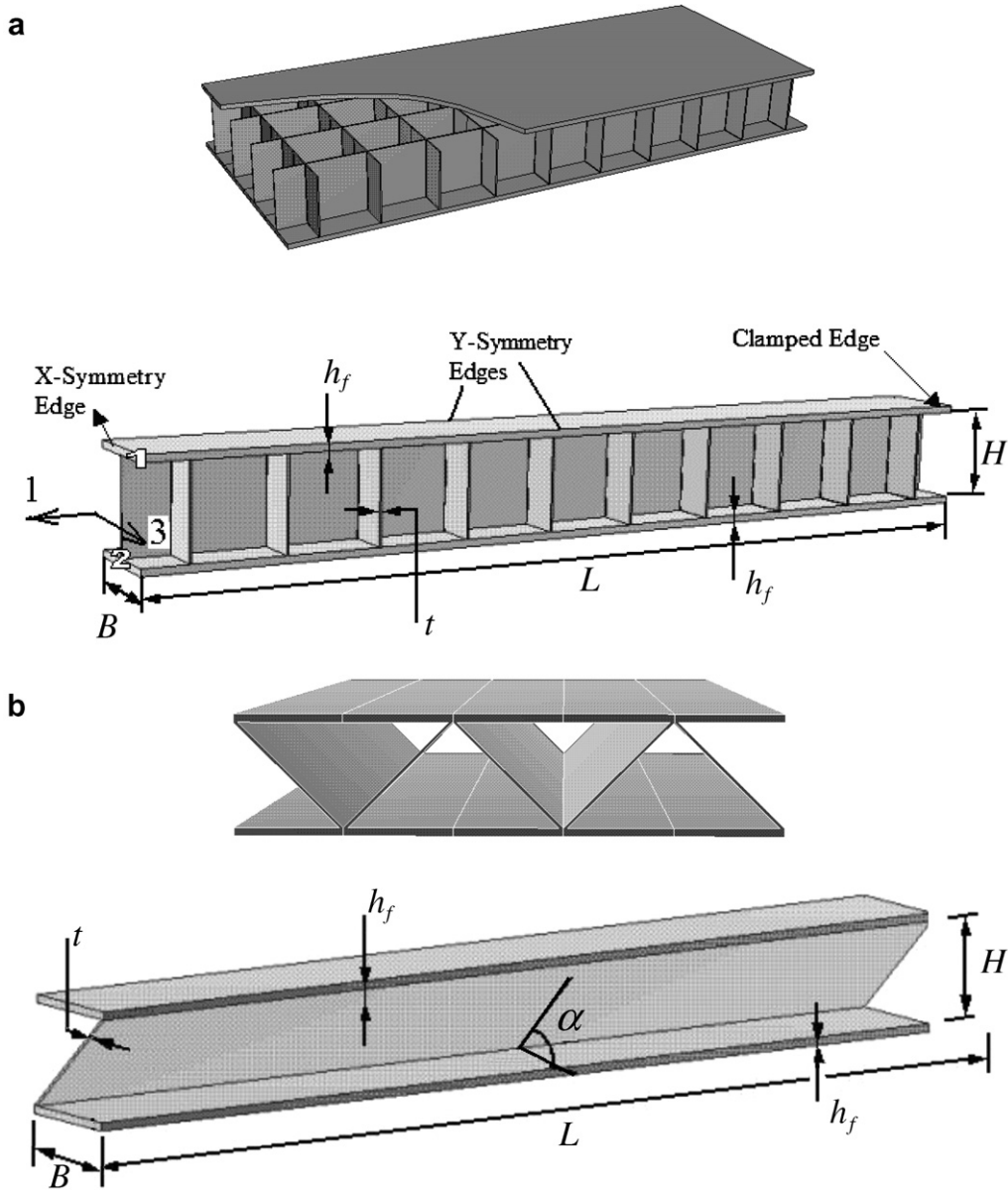


Fig. 3. Schematic diagram of metal sandwich plate configurations and the corresponding computational models for (a) square honeycomb sandwich plate, (b) folded sandwich plate. Plate sections and the periodic basic units employed in the numerical analysis are shown. The plates are infinitely long in one direction with transverse width  $2L$ . The faces and core webs are clamped (welded) to rigid supports along the sides. The basic periodic unit of the sandwich plate, of width  $L$ , exploits symmetry at the center and along the edges perpendicular to the sides.

with Young's modulus  $E = 200$  GPa, Poisson ratio  $\nu = 0.3$ , tensile yield strength  $\sigma_Y = 205$  MPa and strain hardening exponent  $N = 0.17$  (American Society of Metals, 1985). Strain-rate sensitivity of the steel is not taken into account. Classical flow theory based on the Mises yield surface and isotropic hardening is employed in the simulations. It has been assumed that the steel can sustain the strains that arise without fracture due to its high ductility.

Both core topologies have height,  $H$ , web thickness,  $t$ , and face sheet thickness,  $h_f$ . The square honeycomb core has web spacing  $B$ . The folded plate core has an inclination angle,  $\alpha$ , such that the spacing of the folds is  $B = t/\sin\alpha + H/\tan\alpha$ . With  $f_c$  as the relative density of the core (i.e. the volume fraction of the core occupied by the webs), the square honeycomb core has

$$f_c = 2\frac{t}{B} - \left(\frac{t}{B}\right)^2 \cong 2\frac{t}{B} \quad (13)$$

while the folded plate core has

$$f_c = \frac{t}{t + H \cos \alpha} \quad (14)$$

The mass/area of the solid plate is  $M = \rho_P h_{\text{solid}}$ , where  $h_{\text{solid}}$  denotes its thickness; for the sandwich plates,  $M = \rho_P(2h_f + f_c H)$ . If  $L$ ,  $M$  and  $\rho_s$  are specified, the geometry of each of the sandwich plates is fully determined by  $f_c$ ,  $H/L$  and  $B/H$ , or, equivalently, by  $\alpha$  rather than  $B/H$  for the folded plate core.

All the calculations presented in this paper are performed for 304 stainless steel plates with  $M/\rho_P L = 0.02$ ,  $L = 1$  m and  $H/L = 0.1$  for the sandwich plates. The thickness of the solid plate is 20 mm. The square honeycomb cores have  $B/H = 1$ , while the folded cores have  $\alpha = 45^\circ$  such that  $B/H \cong 1$ . The relative density of both the square honeycomb core and the folded plate core is taken to be  $f_c = 0.04$  in most of the examples considered in this section, corresponding to  $h_f = 8$  mm for each face sheet of the sandwich. This set of choices is the same as that chosen as representative of full scale panels in an earlier study, and the parameters characterizing these sandwich plates have been shown to be nearly optimal under air blasts from a minimum weight perspective for plates designed to deflect no more than  $0.2L$  (Hutchinson and Xue, 2005). However, neither of these earlier studies accounted for fluid–structure interaction. The measure of deformation for the solid plate is taken as the maximum deflection,  $\delta$ , at the center of the plate. For the sandwich plates, the maximum center deflection of each face,  $\delta_{\text{top}}$  (towards the blast) and  $\delta_{\text{bottom}}$ , will be presented, together with the average crushing strain at the center,  $\bar{\epsilon}_c$ .

As described in the previous section, calculations based on the *applied pressure approach*, take the pressure history (11) to be applied uniformly to the surface of the plate towards the blast. For the solid plate  $h_P = h_{\text{solid}}$ , while for the sandwich plate  $h_P$  is identified with the thickness of the face sheet,  $h_f$ . In the *prescribed velocity approach*, a uniform initial velocity,  $I/(\rho_P h_{\text{solid}})$ , is imposed on the solid plate and,  $I/(\rho_P h_f)$ , is imposed on the face sheet towards the blast for the sandwich plate. When fluid–structure interaction is taken into account,  $I$  is determined by the KNR formula (5); when it is ignored,  $I$  is taken to be  $I_{m_P \rightarrow \infty}$  from (4). It should be noted that the KNR result for  $I$  does not account for resistance on the back side of the plate—by the air for the solid plate and by the core for the face sheet. This source of error is likely to be more important for the sandwich plate than the solid plate, as will be further discussed in Section 5.

In the simulations presented in this paper, the additional parameter choices are

$$t_0 = 10^{-4} \text{ s}, \quad p_A = 0.1 \text{ MPa}, \quad \rho_A = 1.25 \text{ kg m}^{-3} \quad (c_A = 331 \text{ m s}^{-1}) \quad (15)$$

Once the intensity of the incident blast wave is prescribed, the specification of the plate for each of the two loading approaches is complete. The intensity is measured by the peak pressure,  $p_0$ . The momentum/area transferred to the plate,  $I$ , is then fully determined by (5). Normalization deflections,  $\delta/L$ , and crushing strains,  $\bar{\epsilon}_c$ , will be presented against intensity as measured by  $p_0/p_A$ . The dimensionless time scales setting fluid–structure interaction are indicated in Fig. 4:  $\beta_A = 0.00026$  for the solid plate, and  $\beta_A = 0.00065$  for the face sheet of the sandwich plate.

Calculations have been carried out using ABAQUS Explicit (2001). Sections of the two sandwich plates shown in Fig. 3b are employed with boundary conditions consistent with symmetry and periodicity applied to the edges perpendicular to support wall. Symmetry conditions are applied at the center. The face sheets

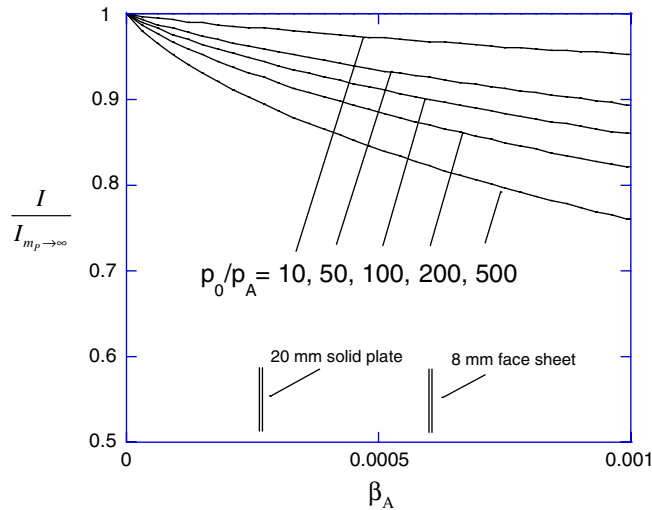


Fig. 4. Momentum/area,  $I$ , transmitted to the solid plate and to the face sheet towards the blast. Values of  $\beta_A$  for the examples studied in Section 3 are indicated. The dimensionless measure of incident blast pulse duration and plate mass/area is  $\beta_A = t_0 \rho_A c_A / (\rho_P h_P)$  and the normalized intensity of the blast is  $p_0/p_A$ . The momentum/area transmitted to the infinitely massive plate,  $I_{m_p \rightarrow \infty}$ , is given by (4). For the solid plate,  $h_P = h_{\text{solid}}$ ; for the sandwich plate,  $h_P = h_f$ .

and core webs intersecting the support wall are modeled as being attached to a rigid surface. Three-dimensional meshing of both the face sheets and the core webs is used as described by Xue and Hutchinson (2004).

Fig. 5 illustrates two of the primary issues investigated in this paper: (i) the extent to which fluid–structure interaction is important in air blasts and (ii) the performance of sandwich plates compared to solid plates. The sandwich plate has a square honeycomb core. All results in this figure were computed using the prescribed velocity approach. For the plates analyzed without accounting for fluid–structure interaction (FSI), the momentum/area,  $I$ , applied to the plate is taken as the value associated with the massive plate limit,  $I_{m_p \rightarrow \infty}$ . Application of  $I_{m_p \rightarrow \infty}$  has been the customary practice in modeling air blasts in calculations which decoupled the structure from the fluid (Fleck and Deshpande, 2004; Xue and Hutchinson, 2004; Qui et al., 2005; Dharmasena et al., in press; Vaziri et al., 2006). As seen in Fig. 4, when FSI is taken into account, the momentum/area,  $I$ , can be as much as 10% below  $I_{m_p \rightarrow \infty}$  for the solid plate and 20% below  $I_{m_p \rightarrow \infty}$  for the sandwich plate at highest blast intensity considered. The effect of the reduced momentum transfer due to FSI is evident in the trends in Fig. 5, including those for the average core crushing strain at the center of the sandwich plate,  $\bar{\epsilon}_c$ , shown in Fig. 5b. In addition, the benefit of less momentum transmitted to the sandwich plate relative to the solid plate is also seen in Fig. 5. However, sandwich construction in these air blasts is not nearly as beneficial as in water blasts causing comparable deflections where the momentum acquired by a sandwich plate can be as little as one half that acquired by the solid plate.

Fig. 6 compares predictions from the two approaches for applying the load for both the solid plate and the sandwich plate with the square honeycomb core. The differences between the deflections from the two approaches are generally quite small, particularly for the solid plate and the bottom face of the sandwich plates where they are almost indistinguishable. The largest difference is reflected in the core crushing strain in Fig. 6b. The difference in  $\bar{\epsilon}_c$  between the two approaches is reflected in the larger top face deflection predicted by the prescribed velocity approach, but the effect is relatively small because  $\bar{\epsilon}_c$  does not exceed 30%. Deformed shapes at two intensities of loading are shown in Fig. 6c.

The corresponding curves showing the outcomes of the two approaches for applying the loading to the sandwich plate with a folded plate core are shown in Fig. 7. The folded plate core is weaker than the square honeycomb. As seen in Fig. 7c, the webs buckle, collapse and make contact with the face sheets. While the square honeycomb core only experiences a crushing strain of 25% at the highest intensity ( $p_0/p_A \cong 200$ ), the folded plate suffers this same level of crushing at  $p_0/p_A \cong 75$ . At blast intensities above  $p_0/p_A \cong 75$ , the buckled webs of folded plate core make contact with the face sheets, increasing the effective collapse strength

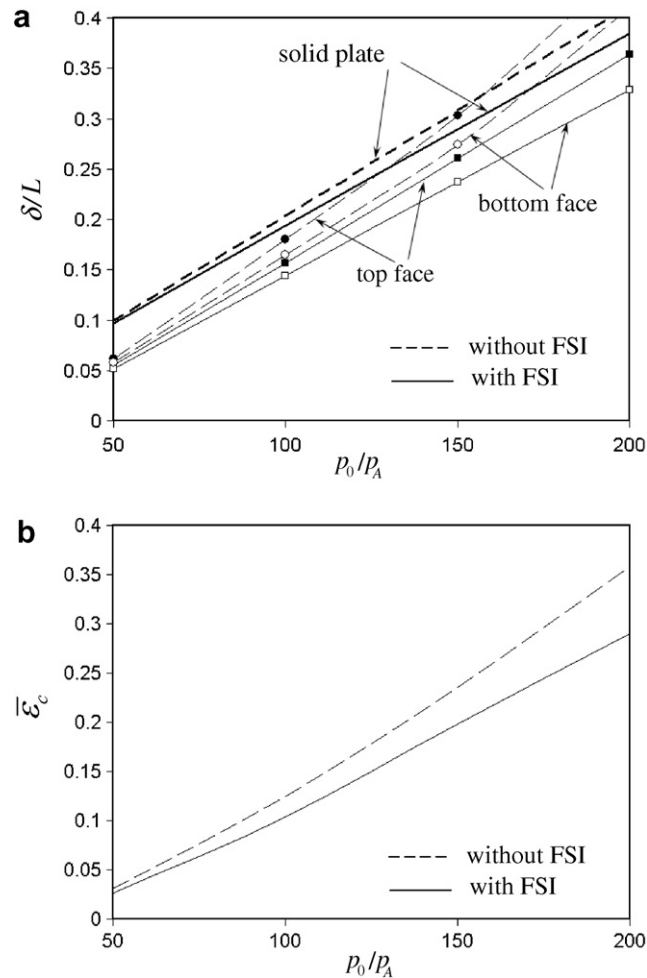


Fig. 5. (a) Normalized maximum deflection of the solid plate and the top and bottom faces of the square honeycomb sandwich plate as a function of  $p_0/p_A$  simulated using the prescribed velocity approach with and without considering the FSI effect. (b) Residual average compressive strain of the core at the middle of square honeycomb,  $\bar{\epsilon}_c$ , as a function of  $p_0/p_A$  with and without considering the FSI effect. The period of the incident pulse is  $t_0 = 10^{-4}$  s.

of the core, as seen in Fig. 7b. Due to core crush, the top face sheet undergoes about as much deflection as the solid plate. However, the bottom face sheet is spared, and it undergoes about the same deflection as the bottom face of the sandwich plate with the square honeycomb core.

A limited study of the optimal design of honeycomb core sandwich plates subject to an air blast is presented in Fig. 8, where a series of calculations have been carried out for plates with the same mass/area,  $M/\rho_p L = 0.02$ , considered in the studies described above. Now, however, mass in the core, as measured by  $f_c$ , is traded against mass in the face sheets with core thickness and web spacing fixed at the same values used in the previous cases, i.e.,  $H/L = 0.1$  and  $B/H = 1$ . Top and bottom face sheets are constrained to have the same thickness. The incident blast pulse has  $p_0/p_A = 100$  with  $t_0 = 10^{-4}$  s. For the prescribed velocity and the applied pressure approaches, the minimum deflection of the top and bottom faces occurs for a core with  $f_c = 0.04$ , although the minimum is shallow. The differences between the two methods for applying the loading are consistent with the results described earlier, with the main difference again being in the amount of core crush. The finding that a core with a relative volume fraction of about 4% is near-optimal for plates with  $H/L = 0.1$  designed to withstand this intensity of air blast is consistent with earlier conclusions based on simulations which ignored fluid–structure interaction (Xue and Hutchinson, 2004; Hutchinson and Xue, 2005).

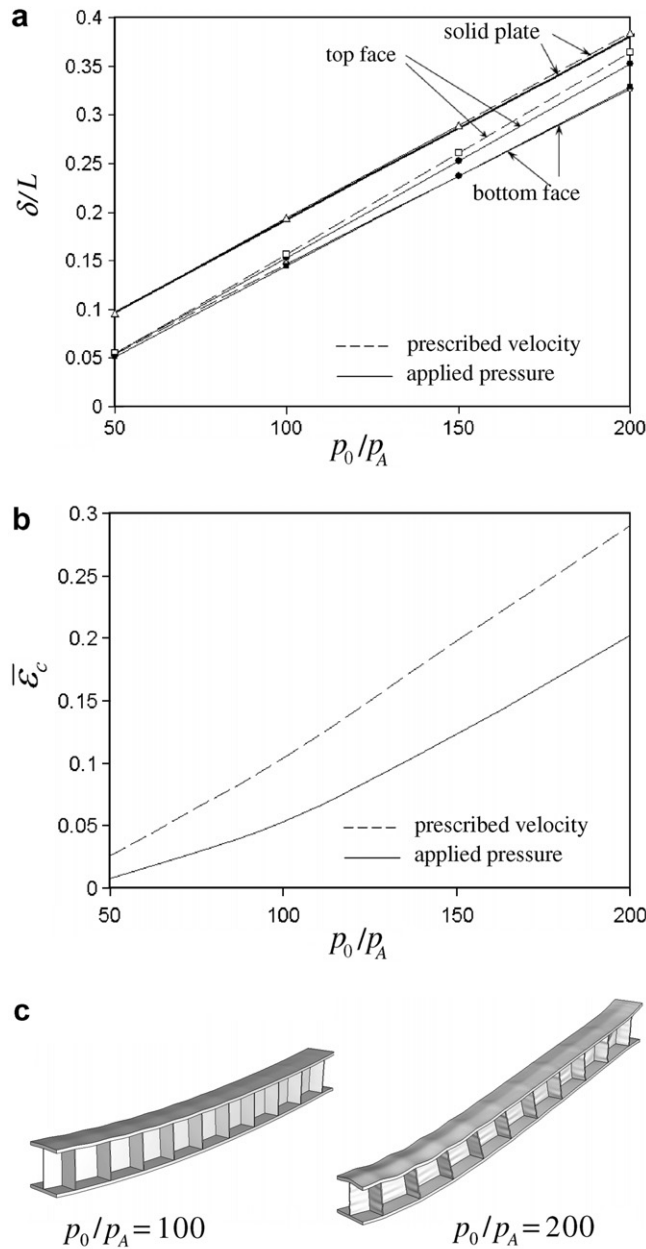


Fig. 6. (a) Normalized maximum deflection of the solid plate and the top and bottom faces of the square honeycomb sandwich plate as a function of  $p_0/p_A$  for two methods of applying loading to the plate: applied pressure and prescribed velocity. The difference between the two methods is indistinguishable for the bottom face. (b) Residual average compressive strain of the core at the middle of square honeycomb plates,  $\bar{\epsilon}_c$ , as a function of  $p_0/p_A$  for the two methods of applying loading. (c) Deformed configurations of the square honeycomb sandwich plate for two normalized peak over-pressure simulated using the applied pressure approach. The period of the incident pulse is  $t_0 = 10^{-4}$  s.

#### 4. Applied pressure versus prescribed velocity: unit cell results for the crushing stage

To further highlight the differences that arise between the two ways of applying the dynamic loading, selected calculations have been made for a unit cell of the sandwich plate (cf. insets in Figs. 9a and 10a). The calculations reveal details of deformation and energy absorption in the faces and core of the sandwich

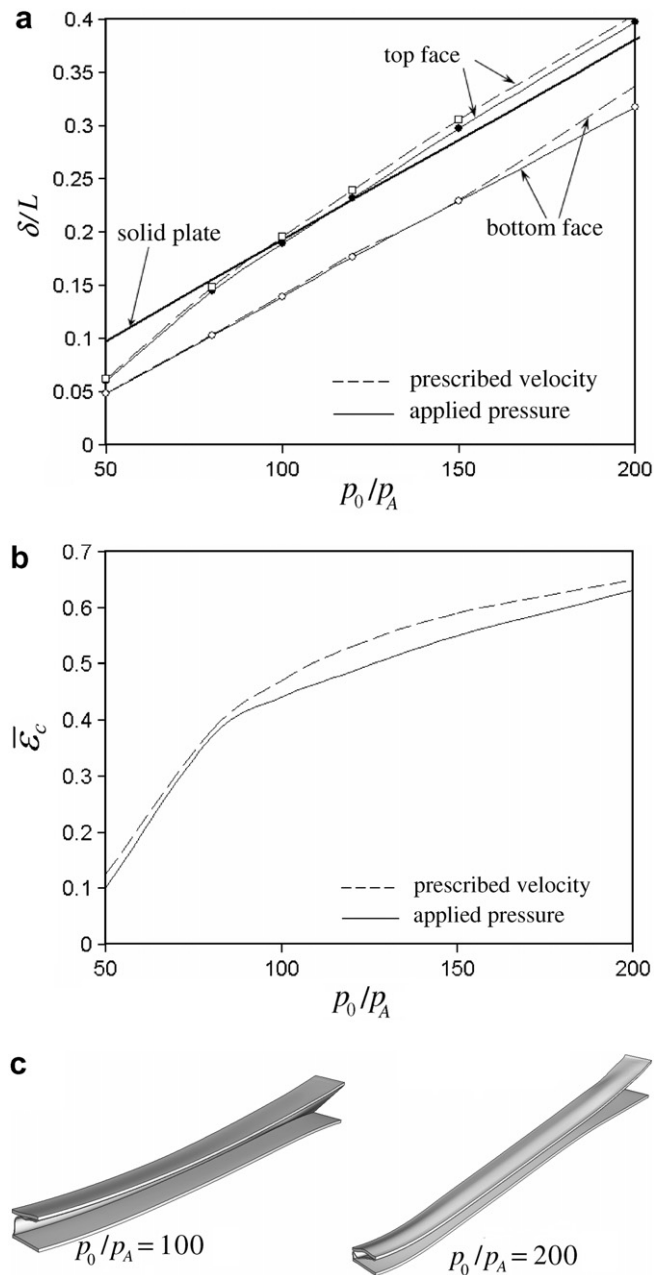


Fig. 7. (a) Normalized maximum deflection of the solid plate and the top and bottom faces of the folded sandwich plate as a function of  $p_0/p_A$  for two methods of applying loading to the plates: applied pressure and prescribed velocity. (b) Residual average compressive strain of the core at the middle of folded plate,  $\bar{\epsilon}_c$ , as a function of  $p_0/p_A$  for the two methods of applying loading. (c) Deformed configurations of the folded sandwich plate for two normalized peak over-pressure simulated using the applied pressure approach. The period of the incident pulse is  $t_0 = 10^{-4}$  s.

plate during the core crushing stage. This is the period of one-dimensional core crushing, designated as Stage II by Fleck and Deshpande (2004), when the plate is imagined to be in free flight and during which the components of the plate acquire a common velocity when crushing ceases. The unit cell is taken as one periodic unit of a plate that is infinite in both directions and which is subject to either the applied pressure history or the initial prescribed velocity. The boundary conditions applied to unit cell on the edges of the face sheets and

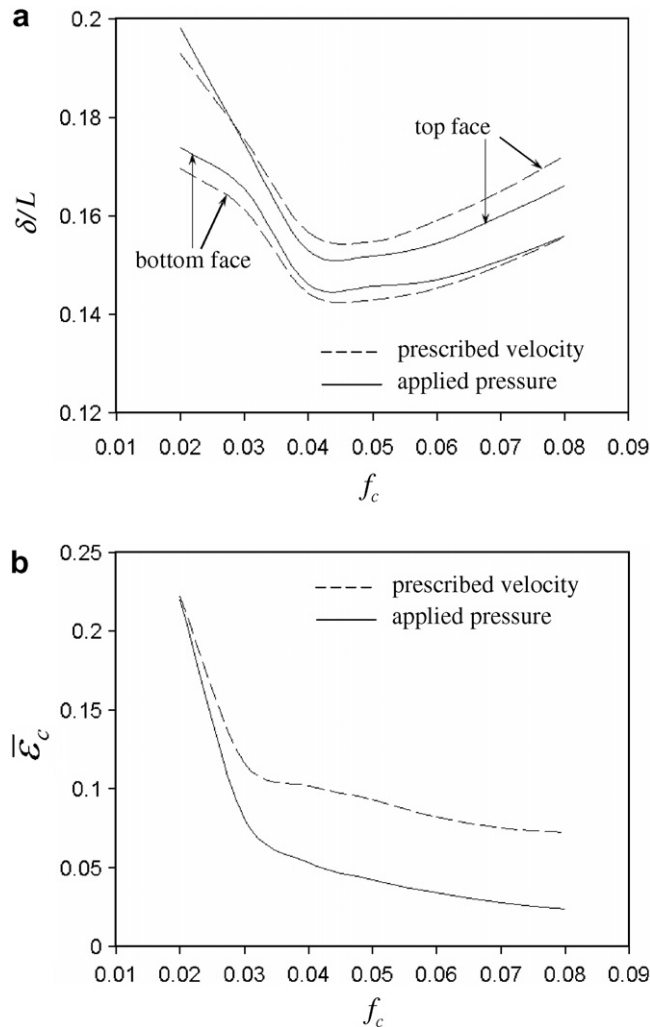


Fig. 8. (a) Normalized maximum deflection of the top and bottom faces of the square honeycomb sandwich plate versus the volume fraction of the core occupied by the webs,  $f_c$ , for two methods of applying loading to the plates: applied pressure and prescribed velocity. (b) Residual average compressive strain of the core at the middle of square honeycomb plates,  $\bar{\epsilon}_c$ , as a function of  $f_c$  for the two methods of applying loading. The incident pulse has the period  $t_0 = 10^{-4}$  s and peak over-pressure  $p_0/p_A = 100$ .

the core webs are consistent with symmetry and periodicity, but the plate is not otherwise constrained in the direction of the overall motion. As in the computations reported in the previous section, the faces and the core webs are fully meshed. The geometry of the plates and the material of which it is made are precisely the same as those specified previously.

For the approach based on prescribed velocity, the initial velocity of the top face is  $I/(\rho_P h_f)$ , such that the initial momentum/area is  $I$ . By conservation of momentum, the common velocity of all components of the sandwich plate is  $I/M$  at the end of the crushing stage, apart from small differences due to elastic vibrations. The initial kinetic energy/area is  $I^2/(2\rho_P h_f)$  while the kinetic energy at the end of crushing is  $I^2/(2M)$ . The energy difference,  $I^2/(2\rho_P h_f) - I^2/(2M)$ , is dissipated in the crushing stage, primarily as plastic dissipation with much smaller amounts as residual elastic energy and vibration energy. The fraction of the initial kinetic energy that must be dissipated during crushing in the prescribed velocity approach is  $\rho_P(h_f + f_c H)/M$ , which is 0.6 for the present examples.

For the applied pressure approach, the pressure acting on the top face is  $p = (I/t_0)e^{-t/t_0}$  with  $t_0 = 10^{-4}$  s, where  $I$  is the same momentum/area as in the prescribed velocity approach. Thus, the final common velocity

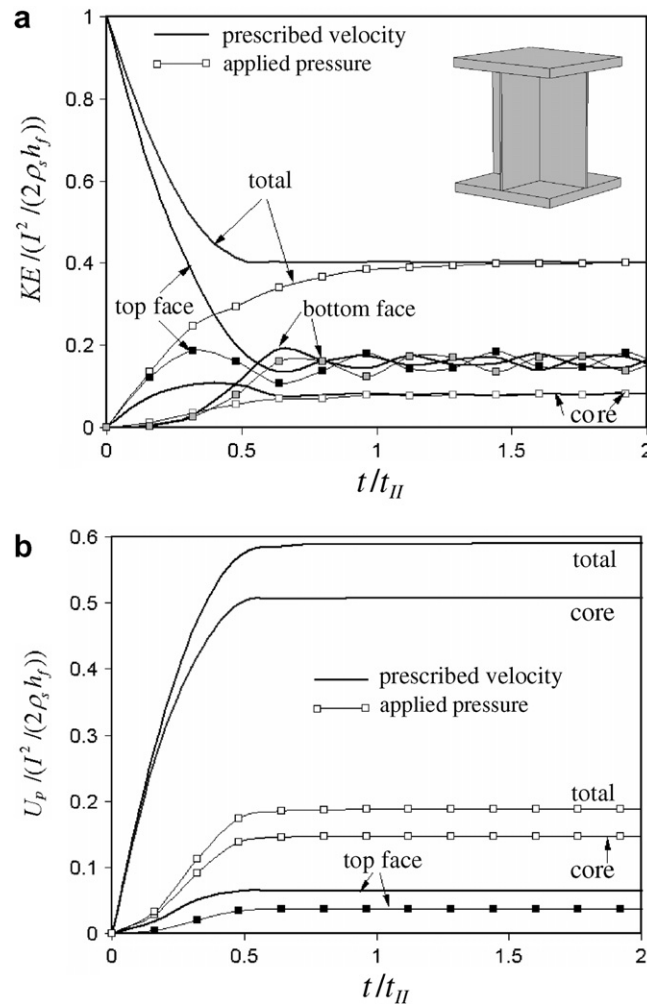


Fig. 9. (a) Time history of normalized kinetic energy in the components of the square honeycomb unit cell calculated based on two methods of applying loading to the plates: applied pressure and prescribed velocity. Inset: schematic diagram of the square honeycomb unit cell. (b) Associated time histories of normalized dissipated energy in the constituents of the unit cell. The square honeycomb has  $M/(\rho_s L) = 0.02$ ,  $f_c = 0.04$ ,  $B/H = 1$  and subject to  $I/(M\sqrt{\sigma_Y/\rho_s}) = 0.25$  with the decay period of  $t_0 = 10^{-4}$  s.

in this approach is also  $I/M$ . However, the initial kinetic energy is zero and the energy that must be dissipated in the crushing stage is not the same as that for the prescribed velocity approach.

The time evolution of the kinetic energy and the plastic dissipation in the faces, in the core, and the total are presented in Fig. 9 for the plate with the square honeycomb core subject to an intense loading with  $I/(M\sqrt{\sigma_Y/\rho_P}) = 0.25$ . The kinetic energy and the plastic dissipation are normalized by the initial kinetic energy imparted to the plate under the prescribed velocity approach,  $I^2/(2\rho_P h_f)$ . The reference time scale used in the normalization in Figs. 9 and 10 is

$$t_{II} = t_0(p_0/\sigma_Y^c) \tag{16}$$

where  $\sigma_Y^c$  is the effective yield strength of the core:  $\sigma_Y^c = f_c \sigma_Y$  for the square honeycomb core and  $\sigma_Y^c = f_c \sigma_Y/2$  for the folded plate core.

Fig. 9 clearly brings out the major differences between the two approaches. In the prescribed velocity approach the kinetic energy of the top face decreases from its initial value with small oscillations as the face asymptotes to the final common velocity. By contrast, the velocity of the top face under the applied pressure

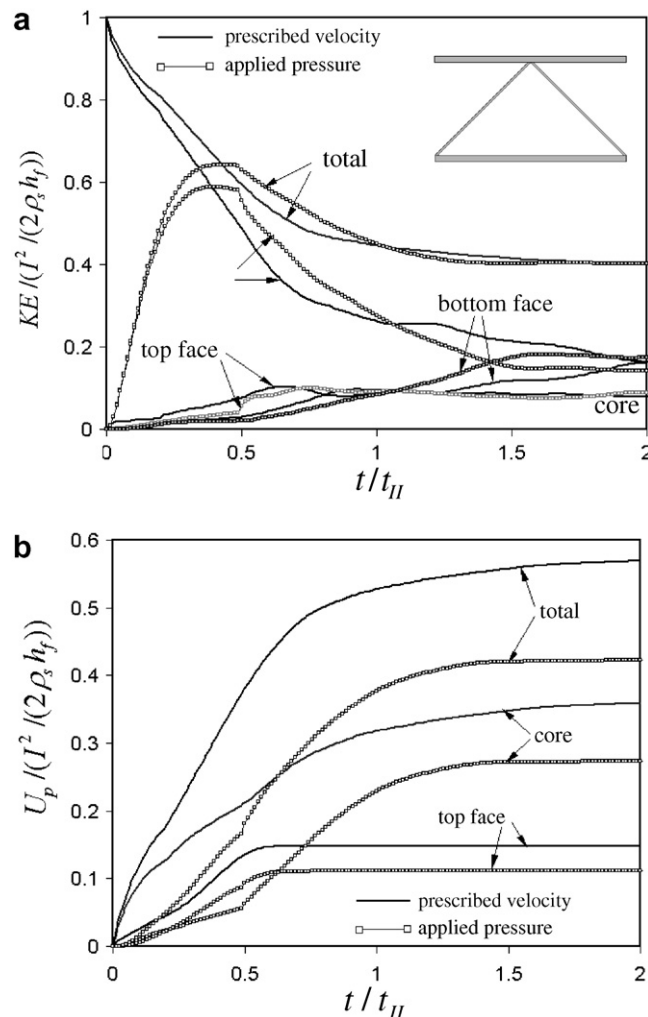


Fig. 10. (a) Time history of normalized kinetic energy in the constituents of the folded plate unit cell calculated based on two methods of applying loading to the plates: applied pressure and prescribed velocity. Inset: schematic diagram of the plane strain model of the folded plate. (b) Associated time histories of normalized dissipated energy in the constituents of the unit cell. The folded core has  $M/(\rho_s L) = 0.02$ ,  $f_c = 0.04$ ,  $\alpha = 45^\circ$  and subject to  $I/(\sqrt{M\sigma_V/\rho_s}) = 0.25$  with the decay period of  $t_0 = 10^{-4}$  s.

approach increases from zero towards the final common velocity. The trends for the total kinetic energy are similar to those for the top face.

More surprising are the large differences between the plastic dissipation under the two approaches seen in Fig. 9b. These trends are consistent with the larger crushing strains produced by the prescribed velocity approach described in the previous section. In this example, the total energy dissipated during the crushing stage under the applied pressure approach is only one third that dissipated under the prescribed velocity approach. Most of the plastic dissipation occurs in the core, but some occurs in the top face sheet due to plastic bending around the core webs. Even though the prescribed velocity approach significantly overestimates crushing dissipation, it leads to relatively small discrepancies in the final back face deflections for clamped plates, as the examples in the previous section illustrate.

Stage II results for sandwich plates with folded plate cores are displayed in Fig. 10. The trends are similar to those for the plates with square honeycomb cores, but the discrepancy between the plastic dissipations predicted by the two approaches is not as great. The folded plate core is not nearly as effective in dissipating plastic deformation in crush as the square honeycomb, and it undergoes significantly larger crushing strains. In addition, the face sheets of the sandwich plate with the folded plate core experience more plastic dissipation.

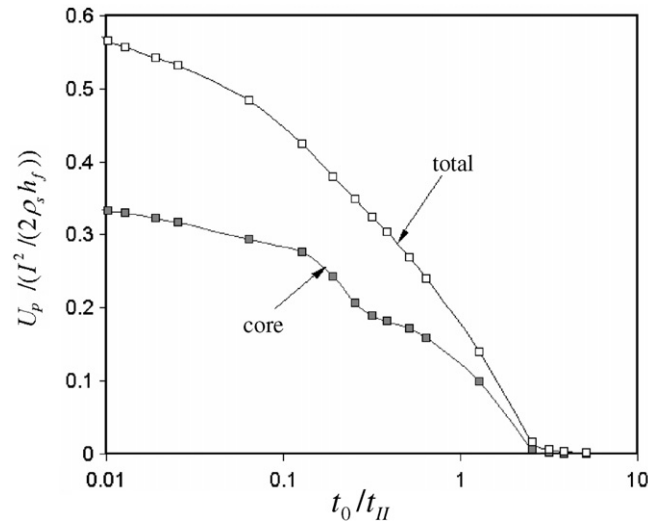


Fig. 11. Normalized plastic energy dissipated in the core along with the total plastic energy dissipated in the unit cell during Stage II of deformation versus the normalized pulse decay period,  $t_0/t_{II}$ . The calculations are based on the applied pressure approach. The folded plate core has  $\bar{M}/(\rho_s L) = 0.02$ ,  $v_s = 0.04$ ,  $\alpha = 45^\circ$  and subject to  $I/(M\sqrt{\sigma_Y/\rho_s}) = 0.25$ .

The role of the period of the pressure pulse,  $t_0$ , in the applied pressure approach on plastic dissipation in the crushing stage is seen in Fig. 11 for the plate with the folded plate core. Here,  $t_0$  is varied while the impulse/area is fixed at  $I/(M\sqrt{\sigma_Y/\rho_p}) = 0.25$ . If  $t_0/t_{II}$  is greater than about 3, the pressure pulse accelerates the plate to the common velocity  $I/M$  without inducing any plastic deformation. Constraint due to plate supports is ignored in these calculations and is likely to become important for large  $t_0$ . By contrast, if  $t_0/t_{II} \cong 0.01$ , the total plastic dissipation and that in the core in Fig. 11 are nearly those associated with the prescribed velocity approach. The value of  $t_0/t_{II}$  associated with the results presented previously in Fig. 10 is 0.065, which is representative for an air shock.

## 5. Conclusions

The present study of all-metal sandwich plates subject to intense air blasts has exploited the new results of Kambouchev et al. (in press) to provide the momentum/area transmitted to the face of the sandwich towards the blast in terms of its mass/area. Typically, for meter-scale panels subject to a heavy air blast, there is a reduction in momentum transfer between 10% and 20% below that for infinitely massive plates. Similarly, there is extra benefit on the order of 10% attributable to fluid–structure interaction for sandwich plates compared to solid plates having the same mass/area. The effects of fluid–structure interaction would be larger for more intense blasts and/or for blast pulses with periods longer than  $t_0 = 10^{-4}$  s (cf. Fig. 1). Nevertheless, the specific examples considered here substantiate the presumption invoked in earlier work that momentum reduction due to fluid–structure interaction is not as important in the design of metal plates against air blasts as against water blasts. The benefits of sandwich plates over solid plates seen in Figs. 6 and 7 are representative for air blasts with  $t_0 = 10^{-4}$  s. While the present study is far from exhaustive, it appears that cores such as the square honeycomb perform better than folded plate cores due to their ability to maintain a high crushing strength at relatively large crushing strains. However, this conclusion should be confirmed for other support conditions with fracture taken into account. By contrast, in water blasts, plate designs with weak cores can more effectively exploit the benefits of fluid–structure interaction than plates with strong cores (Liang et al., in press), at least in the range of intermediate blast intensities.

Like the Taylor theory for water blasts, KNR fluid–structure interaction theory allows the analyst to decouple blast wave propagation in air from the dynamic analysis of the plate for plates struck by planar incident waves. This paper considers two ways to load the plate based on the results of KNR theory. The most

realistic is the applied pressure approach which directly applies to the plate the time-dependent pressure of the reflected wave given by the theory. A simpler approach, called the prescribed velocity approach, which has been more widely used in the past, sets the plate, or face sheet, in motion with an initial velocity chosen to reproduce the momentum/area predicted by KNR theory. There is little difference between the overall deflections of the bottom face of the plates from the two approaches for meter-scale panels subject to air blasts with  $t_0 = 10^{-4}$  s. The greatest difference arises in core crushing. The initial velocity approach can significantly overestimate core crushing and energy dissipation.

As noted in the body of the report, the KNR result for the momentum transmitted to the face sheet towards the blast neglects resistance of the core on the back side of the face sheet. The consequence is that somewhat more momentum will be transmitted to the face than the KNR formula predicts. Further extension of the KNR theory to include such resistance would clarify this aspect.

## Acknowledgements

This work has been supported in part by the ONR under grants N00014-02-1-0700 and GG10376-114934 and in part by the Division of Engineering and Applied Sciences, Harvard University. The authors are indebted to N. Kambouchev, L. Noels and R. Radovitzky for discussions related to KNR theory.

## References

- ABAQUS/Explicit User's Manual, 2001. Version 6.0. Hibbit, Karlsson and Sorensen Inc.
- American Society of Metals, 1985. In: Boyer, H.E., Gall, T.L., (Eds.), *Metals Handbook Desk Edition*.
- Dharmasena, K.P., Wadley, H.N.G., Xue, Z., Hutchinson, J.W., in press. Mechanical response of metallic honeycomb sandwich panel structures to high intensity dynamic loading. *Int. J. Impact Eng.*
- Fleck, N.A., Deshpande, V.S., 2004. The resistance of clamped sandwich beams to shock loading. *J. Appl. Mech.* 71, 386–401.
- Hutchinson, J.W., Xue, Z., 2005. Metal sandwich plates optimized for pressure impulses. *Int. J. Mech. Sci.* 47, 545–569.
- Kambouchev, N., Noels, L., Radovitzky, R., 2006. Compressibility effects in fluid–structure interaction and their implications on the air-blast loading of structures. *J. Appl. Phys.* 100, 063519.
- Liang, Y., Spuskanyuk, A.V., Flores, S.E., Hayhurst, D.R., Hutchinson, J.W., McMeeking, R.M., Evans, A.G., in press. The response of metal sandwich panels to water blasts. *J. Appl. Mech.*
- Qui, X., Deshpande, V.S., Fleck, N.A., 2005. Finite element analysis of the dynamic response of clamped sandwich beam subject to shock loading. *Eur. J. Mech./Solids A* 22, 801–814.
- Rabczuk, T., Kim, J.Y., Samaniego, E., Belytschko, T., 2004. Homogenization of sandwich structures. *Int. J. Numer. Meth. Eng.* 61, 1009–1027.
- Rathbun, H.J., Radford, D.D., Xue, Z., He, M.Y., Yang, J., Deshpande, V., Fleck, N.A., Hutchinson, J.W., Zok, F.W., Evans, A.G., 2006. Performance of metallic honeycomb-core sandwich beams under shock loading. *Int. J. Solids Struct.* 43, 1746–1763.
- Taylor, G.I., 1963. The pressure and impulse of submarine explosion waves on plates. In: Batchelor, G.K. (Ed.), *The Scientific Papers of Sir Geoffrey Ingram Taylor, Volume III: Aerodynamics and the Mechanics of Projectiles and Explosions*. Cambridge University Press, pp. 287–303.
- Vaziri, A., Xue, Z., Hutchinson, J.W., 2006. Metal sandwich plates with polymeric foam-filled cores. *J. Mech. Mater. Solids* 1, 95–128.
- Xue, Z., Hutchinson, J.W., 2004. A comparative study of impulse-resistant metallic sandwich plates. *Int. J. Impact Eng.* 30, 1283–1305.